

Technical note

# Mathematical modelling of stress in the hip during gait

M. Ipavec<sup>a</sup>, R.A. Brand<sup>b</sup>, D.R. Pedersen<sup>b</sup>, B. Mavčič<sup>a</sup>, V. Kralj-Iglič<sup>c</sup>, A. Iglič<sup>a,\*</sup>

<sup>a</sup>Laboratory of Applied Physics, Faculty of Electrical Engineering, University of Ljubljana, Ljubljana, Slovenia

<sup>b</sup>Department of Orthopaedic Surgery, University of Iowa, Iowa City, USA

<sup>c</sup>Institute of Biophysics, Medical Faculty, University of Ljubljana, Ljubljana, Slovenia

Received 18 November 1997; accepted 6 June 1999

## Abstract

A mathematical model is developed for calculating the contact stress distribution in the hip for a known resultant hip force and characteristic geometrical parameters. Using a relatively simple single nonlinear algebraic equation, the model can be readily applied in clinical practice to estimate the stress distribution in the most frequent body positions of everyday activities. This is demonstrated by analyzing the data on the resultant hip force obtained from laboratory observations where a stance period of gait is considered. © 1999 Elsevier Science Ltd. All rights reserved.

*Keywords:* Contact stress; Resultant hip force; Inverse dynamics; Gait; Muscle forces

## 1. Introduction

The distribution of contact stress in the hip is an important factor which affects the development of the hip and also determines the state of health or disease of the adult hip (Pauwels, 1976; Brinckmann et al., 1981; Kummer, 1991; Hadley et al., 1990; Maxian et al., 1995; Baker et al., 1989; Krebs et al., 1991).

Direct measurements would record contact stresses in the most realistic manner. The contact stress distribution in the hip was measured directly by an instrumented device, first in vitro (Rushfeldt et al., 1981; Brown and Shaw, 1983) and later in vivo (Hodge et al., 1986, 1989). These measurements give insight also into the features of the intact hip. It should, however, be borne in mind that metal transducers or implant surfaces do not preserve the natural cartilage microstructure and natural fluid film lubrication so that predicted contact stresses may differ from the natural ones. These approaches also measure contact stresses at discrete locations, rather than overall. For non-operated patients, external laboratory measurements in combination with simulations or mathematical models can make global predictions. Contact finite element simulations (Rapperport et al., 1985; Brown et al.,

1993; Dalstra and Huijskes, 1995) provide complete distributions, but are complex and time consuming. Therefore, simpler mathematical models (Legal et al., 1980; Brinckmann et al., 1981; Maxian et al., 1995; Genda et al., 1995) may be adequate for estimating global contact stress distribution in routine surgical planning (Legal et al., 1980; Iglič et al., 1993), provided that they include the relevant phenomena of the particular case.

In the previously reported three-dimensional model (Iglič et al., 1993) we assumed that articular cartilage exhibits ideally elastic behavior and adopted a cosine function for the stress distribution (Greenwald and O'Connor, 1971; Brinckmann et al., 1981). We assumed that the resultant hip force lies in the frontal plane of the body. The present work was intended to generalize the model (Iglič et al., 1993) to the cases of an arbitrary direction of the resultant hip force. We ascertained the sensitivity of the model predictions to the various resultant hip forces during level gait.

## 2. Materials and methods

### 2.1. Mathematical model

The origin of the rectangular Cartesian coordinate system coincides with the center of the right hip. The coordinate system is oriented so that  $x$ - and  $z$ -axis lie in the frontal plane through the centers of both hips. The

\* Corresponding author. Tel.: + 386-61-1250-278; fax: + 386-61-1264-630.

E-mail address: ales.iglic@fe.uni-lj.si (A. Iglič)

$z$ -axis is vertical, the  $x$ -axis points in the lateral–medial direction, while the  $y$ -axis points in the anterior–posterior direction. The resultant hip contact force  $\mathbf{R}$  originates in the center of the femoral head. The articular surface is described as a part of the spherical surface with a radius the mean of the radii of the femoral head and acetabular subchondral bone. The femoral head and the acetabulum are in contact over the hemisphere defined by the acetabular shell. The tangential stress due to frictional forces is assumed negligible compared to the corresponding normal stress (Legal et al., 1980). These assumptions can be justified for smooth, well lubricated femoral and acetabular surfaces which are almost spherical and congruent and subject to extremely low coefficients of friction;  $\simeq 0.001$  (Shrive and Frank, 1995).

Using the spherical coordinate system originating in the center of the articular sphere, the radius vector of an arbitrary point on the articular surface is given by  $\mathbf{r} = (r \cos \varphi \sin \vartheta, r \sin \varphi \sin \vartheta, r \cos \vartheta)$ , where  $r$  is the radius of the articular sphere,  $\varphi$  is the azimuthal angle and  $\vartheta$  is the polar angle. The resultant hip force is given by the vector  $\mathbf{R} = (R \sin \vartheta_{\mathbf{R}} \cos \varphi_{\mathbf{R}}, R \sin \vartheta_{\mathbf{R}} \sin \varphi_{\mathbf{R}}, R \cos \vartheta_{\mathbf{R}})$ , where  $R$  is the magnitude of the resultant hip force,  $\vartheta_{\mathbf{R}}$  is the inclination of the direction of the resultant hip force with respect to the vertical axis and  $\varphi_{\mathbf{R}}$  is the angle of rotation of the direction of the resultant hip force in the horizontal plane (from the positive  $x$ -axis in the counterclockwise direction).

The contact stress integrated over the weight bearing area  $S$  yields the resultant hip force  $\mathbf{R}$ ,

$$\int_S p \, d\mathbf{S} = \mathbf{R}, \quad (1)$$

where  $d\mathbf{S} = (\sin \vartheta \cos \varphi, \sin \vartheta \sin \varphi, \cos \vartheta) r^2 \sin \vartheta \, d\vartheta \, d\varphi$ .

Based on the assumption that the radial stress on the articular surface of the hip is proportional to the radial strain of the cartilage layer, the radial stress is proportional to the cosine of the angle between that point and the position of the stress pole ( $\gamma$ ) (Greenwald and O'Connor, 1971; Brinckmann et al., 1981),

$$p = p_0 \cos \gamma, \quad (2)$$

where  $p_0$  is the value of stress at the pole (the point where the distance between the acetabular sphere and the femoral head sphere would be minimal; Brinckmann et al., 1981). Cosine of the angle  $\gamma$  can be written as

$$\cos \gamma = \sin \Theta \sin \vartheta \cos \Phi \cos \varphi + \sin \Theta \sin \vartheta \sin \Phi \sin \varphi + \cos \vartheta \cos \Theta, \quad (3)$$

where the polar angle  $\Theta$  determines the angular displacement of the pole from the vertical axis, while the azimuthal angle  $\Phi$  describes the angular displacement of the pole in the horizontal plane from the  $x$ -axis in the counterclockwise direction.

The weight bearing area  $S$  is defined as a part of the articular sphere constrained by the acetabular geometry as well as the position of the stress pole. The lateral border of the weight bearing area, determined by the acetabular geometry, may be visualized as an intersection of the articular sphere with a plane passing through the center of the sphere and being inclined by the CE angle of Wiberg ( $\vartheta_{\text{CE}}$ ) (Wiberg, 1939) with respect to the vertical body axis. Since only the positive values of stress have a physical meaning, the medial border of the weight bearing area which is dependent on the position of the pole of stress, is determined as the line where stress (Eq. (2)) vanishes, so that

$$\cos \gamma = 0. \quad (4)$$

The medial border of the weight bearing area determined by the condition (4) consists of all the points that lie  $\pi/2$  away from the pole of stress and may likewise be visualized as an intersection of the articular sphere with a plane passing through the center of the sphere, the inclination of this plane being determined by the location of the stress pole. As both intersection planes which confine the weight bearing area are passing through the center of the sphere they both form circles of radii  $r$  at the intersection of the plane and the articular sphere. The weight bearing area is therefore confined by these two intersecting circles on the articular sphere.

The stress distribution in a given body position is calculated by solving the three components of the vector equation (1) where Eqs. (2)–(4) are taken into account,

$$\vartheta_{\mathbf{R}} + \Theta \mp \arctan \left( \cos^2 (\vartheta_{\text{CE}} - \Theta) \left/ \left( \pi \pm \left[ \frac{\pi}{2} - \vartheta_{\text{CE}} + \Theta - \frac{1}{2} \sin(2 \cdot (\vartheta_{\text{CE}} - \Theta)) \right] \right) \right) \right) = 0, \quad (5)$$

$$p_0 = \frac{3R}{2r^2} \cos(\vartheta_{\mathbf{R}} + \Theta) \left/ \left( \pi \pm \left[ \frac{\pi}{2} - \vartheta_{\text{CE}} + \Theta - \frac{1}{2} \sin(2 \cdot (\vartheta_{\text{CE}} - \Theta)) \right] \right) \right). \quad (6)$$

$$\Phi = \varphi_{\mathbf{R}} \text{ or } \Phi = \varphi_{\mathbf{R}} \pm \pi. \quad (7)$$

Here, the upper sign stands for the case when the pole lies on the lateral side of the contact hemisphere or outside the contact hemisphere in the lateral direction and the lower sign stands for the case when the pole lies on the medial side of the contact hemisphere or outside the contact hemisphere in the medial direction. The procedure for obtaining the Eqs. (5)–(7) and the description of the weight bearing area are briefly described in Appendix A.

The value of  $\Theta$  corresponding to the Eq. (5) was determined by the Newton iteration method. Here the validity of Eq. (5) was ensured up to the precision of  $\varepsilon < 10^{-10}$ . The value of  $p_0$  is expressed from Eq. (6) using

the obtained  $\Theta$ . If  $\Theta$  is negative,  $\Phi$  should be in the interval between  $-\pi/2$  and  $\pi/2$  while if it is positive,  $\Theta$  should be in the interval between  $\pi/2$  and  $3\pi/2$ .

By knowing the magnitude and the direction of the resultant hip force, the CE angle and the radius of the articular sphere, the value of stress at the pole and the position of the pole can be determined from the Eqs. (5)–(7). The stress distribution on the weight bearing area is then calculated by Eqs. (2) and (3).

If the pole of the stress distribution is located within the weight bearing area, the location of the maximum stress ( $p_{\max}$ ) coincides with the location of the pole, and in this case  $p_{\max}$  equals  $p_0$  (Fig. 1A,C,D). However, when the stress pole lies outside the weight bearing area, the stress on the weight bearing area is maximal at that point on the weight bearing area which is the closest to the pole (Fig. 1B).

## 2.2. Determination of the hip resultant force during gait

The hip resultant force  $\mathbf{R}$  was determined in different phases of a stance period of gait of a person with an implanted total hip endoprosthesis as previously described (Brand et al., 1994; Crowninshield et al., 1978). The values of  $\mathbf{R}$ ,  $\vartheta_R$  and  $\varphi_R$  were determined in the coordinate system fixed with respect to the pelvis (Brand et al., 1994) so that the calculated stress distribution (Figs. 2 and 3) represents the loading of the acetabulum.

## 3. Results

The stress distribution and its maximal value  $p_{\max}$  change as the weight bearing area changes due to the variation of the inclination of the resultant force  $\vartheta_R$ . The lowest value of  $p_{\max} = 3R/2\pi r^2$  is obtained when the direction of the resultant force  $\mathbf{R}$  is inclined for an angle  $\pi/2$  in the medial direction from the lateral acetabular border ( $\vartheta_R + \vartheta_{CE} = \pi/2$ ) since in this case the weight bearing area is the maximal possible, i.e. it covers the whole contact (acetabular) hemisphere.

When the resultant force  $\mathbf{R}$  is inclined away from this central direction (where  $\vartheta_R + \vartheta_{CE} = \pi/2$ ), the size of the weight bearing area decreases, while the pole is shifted towards the respective border of the weight bearing area. For large inclinations of  $\mathbf{R}$  from the central position, the pole is located outside of the weight bearing area while the stress attains its maximal value on the acetabular rim. The coordinate of the pole  $\Theta$  monotonically decreases with increasing  $\vartheta_R$ . The value of  $p_{\max}$  is considerably increased when the pole lies outside the weight bearing area. At the limits where  $\vartheta_R + \vartheta_{CE}$  approach 0 or  $\pi$ , the weight bearing area vanishes, the peak stress increases beyond a limit while the pole lies for  $\pi/2$  away from the edge of the articular hemisphere rim.

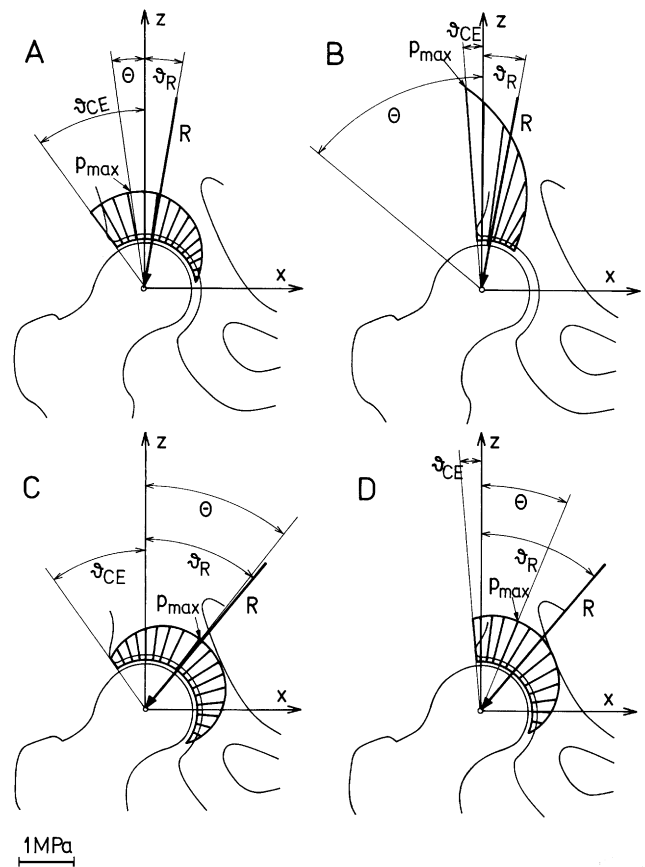


Fig. 1. The calculated distribution of stress in the hip joint for different values of the CE angles and  $\vartheta_R$ :  $\vartheta_R = 10^\circ$ ,  $\vartheta_{CE} = 35^\circ$  (A),  $\vartheta_R = 10^\circ$ ,  $\vartheta_{CE} = 5^\circ$  (B),  $\vartheta_R = 40^\circ$ ,  $\vartheta_{CE} = 35^\circ$  (C),  $\vartheta_R = 40^\circ$ ,  $\vartheta_{CE} = 5^\circ$  (D). The values of the other model parameters are:  $R = 2000$  N,  $\varphi_R = 0$  and  $r = 2.6$  cm.

When CE angle and  $\vartheta_R$  are both small, the pole lies outside the weight bearing area which is substantially diminished (Fig. 1B). This latter situation is analogous to that with dysplastic hips. Cases A and D (Fig. 1) have equal ( $\vartheta_{CE} + \vartheta_R$ ), i.e. they have the same angle between the lateral rim of the acetabulum and the direction of the force  $\mathbf{R}$ , and therefore equal shape of the stress distribution. The two distributions, however, differ in their position with respect to the coordinate system of the body.

In the case of larger CE angle ( $\vartheta_{CE} = 35^\circ$ ) the pole of the stress distribution lies within the weight bearing area in all phases of the stance period of gait so that the location of the maximal stress coincides with the location of the stress pole ( $p_{\max} = p_0$ ) (Fig. 2). In the case of smaller CE angle ( $\vartheta_{CE} = 5^\circ$ ) the values of  $p_{\max}$  are considerably increased with respect to the corresponding values pertaining to  $\vartheta_{CE} = 35^\circ$  (Fig. 2). In one phase of gait the stress pole lies outside the weight bearing area. This point corresponds to the highest  $p_{\max}$  attained in the whole stance period of gait for  $\vartheta_{CE} = 5^\circ$  (Figs. 2 and 3).

Our analysis shows that for various values of the CE angle in nearly all phases during gait the contact stress is

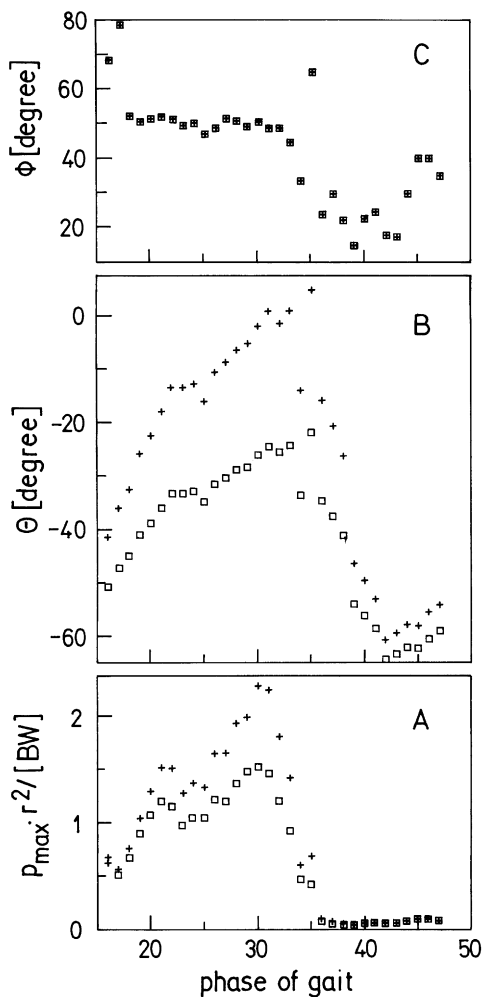


Fig. 2. The calculated maximal stress on the weight bearing area  $p_{\max}$  (A), the coordinate of the stress pole  $|\theta|$  (B) and the coordinate of the stress pole  $\Phi$  (C) in successive phases of the stance period of gait for two values of CE angle:  $\vartheta_{\text{CE}} = 5^\circ$  (+) and  $\vartheta_{\text{CE}} = 35^\circ$  ( $\square$ ). The time interval between the respective phases is 0.04 s, BW is the body weight force. The value of  $p_{\max}$  is determined from Eqs. (5) and (6),  $\theta$  is calculated by solving the nonlinear Eq. (5), while  $\Phi$  is according to Eq. (7) identical to  $\vartheta_{\text{R}}$ . The values of the input data  $R$ ,  $\vartheta_{\text{R}}$  and  $\varphi_{\text{R}}$  are determined as it is described in the second section of the Materials and Methods.

the highest in the superior posterior region of the acetabulum, mostly on the medial side of the femoral head ( $-65^\circ < \theta < 5^\circ$ ,  $15^\circ < \Phi < 80^\circ$ , Figs. 2 and 3). The calculated regions of the highest stresses (Fig. 3) correspond well to the sites of degenerative changes in the acetabulum that have been observed in studies on cadavera (Byers et al., 1974; Das De et al., 1985).

#### 4. Discussion

An analysis of AP radiographs of healthy and dysplastic human hips by using a simple two-dimensional mathematical model of the hip articular stress (Legal and

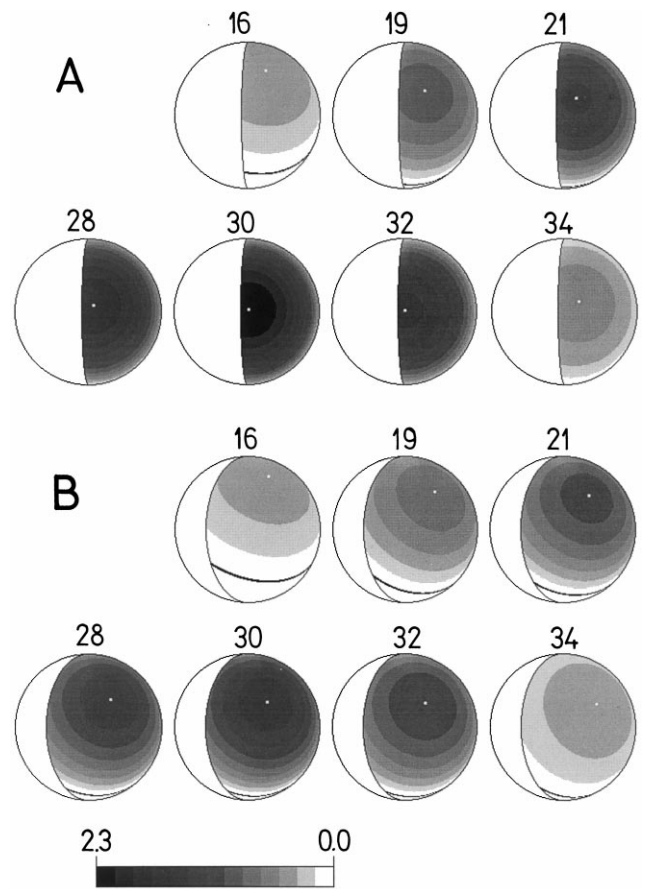


Fig. 3. The contact stress distribution projected onto horizontal plane in the pelvic coordinate system for two values of CE angle:  $\vartheta_{\text{CE}} = 5^\circ$  (A) and  $\vartheta_{\text{CE}} = 35^\circ$  (B). Selected phases of the stance period of gait (marked by the corresponding numbers) are shown. The stress is measured in the units  $\text{BW}/r^2$ , where BW is the body weight force. The location of the stress pole is marked by the white dot.

Ruder, 1977) showed that for a healthy human hip (corresponding to large enough CE angle) the calculated peak stress varied slowly in a large interval of directions of the resultant force exerted by the hip muscles, while in a dysplastic hip (corresponding to small CE angle) the peak stress may have varied considerably more with the direction of the resultant force exerted by the hip muscles. Similarly, the present study shows that in healthy hips having larger CE angle  $p_{\max}$  changes slowly upon the change of the direction of the resultant hip force ( $\vartheta_{\text{R}}$ ), while in the dysplastic hips its value changes considerably upon the change of  $\vartheta_{\text{R}}$ .

The calculated stress distribution in the hip can be considered as a rough estimate. Several simplifications were introduced in the model. First, the cartilage was described macroscopically as a homogenous continuum and a linear elastic solid of a uniform thickness. We did not take into account the specific molecular structure of the glycoprotein bilayer where the two layers are adsorbed on the cartilage of both contact surfaces, nor the role of the intermediate thin fluid film and molecular

structure of the cartilage giving rise to the electrostatic forces (Buschmann and Grodzinsky, 1995). These mechanisms could be realistically described only by using the methods on the molecular level, e.g. the methods of polymer physics and statistical physics. Second, the weight bearing area will be overestimated as a result of not accounting for the cotyloid notch. However, this region would not be expected to actually distribute much load (Figs. 1 and 3). Therefore, the actual underestimation of stress distribution as a result of overestimating contact area is not linearly related and would be anticipated to be negligible.

Due to these simplifications we cannot accurately predict local contact stresses in detail or an absolute stress distribution. However the model predicts global averages which are in accordance with the relevant experimental *in vivo* data in the literature (Hodge et al., 1986,1989; Krebs et al., 1991). These measurements demonstrate that the contact stress in the hip is nonuniform as predicted by our model (Fig. 3). Moreover, the shape of the weight bearing area of the metal–cartilage surface indicated by the values of stress obtained from the transducers of the built-in device in the stance period of gait may be in a rough fashion considered to correspond to the apple-slice surface shape obtained by our model. When gait had normalized (about two years after the implantation of the partial endoprosthesis) the highest measured value of stress during gait reached 4 MPa (Hodge et al., 1989; Krebs et al., 1991). We found a value of peak stress in the stance period of gait around 3 MPa for the normal values of  $r$ ,  $\vartheta_{CE}$  and body weight BW which corresponds well to the above experimental values. It can be concluded that the general features of our model correspond to these measurements.

The cosine radial stress distribution function (Greenwald and O'Connor, 1971; Brinckmann et al., 1981) adopted in this work is based on the assumption that the radial stress in the hip articular surface can be calculated according to Hooke's law (Legal et al., 1980), i.e. the radial stress in the articular surface of the hip is assumed to be proportional to the radial strain of the cartilage layer. In addition, the femoral head and the acetabular shell are taken to be spherical, while the thickness of the cartilage layer before the deformation is assumed to be constant. In normal hips the femoral head and the acetabulum are out-of-round by 1–3 mm. This deviation from the sphericity is even larger in some abnormalities of the hip, where an accurate computation of the contact stress distribution would also be of interest. Since the validity of the cosine stress distribution function used in this work is based on the assumption that the femoral head and the acetabulum have spherical geometry, the deviation from this situation would in general lead to the stress distribution function different from a cosine function (Greenwald and O'Connor, 1971). When the deviation from sphericity is small the contact stress distribu-

tion could be described as a perturbation to the cosine function. It can be shown that in the case of the articular surface having the shape of a rotational ellipsoid with the semiaxes  $r$  and  $(r + \Delta r)$ , respectively, the perturbation of the first order in  $\Delta r/r$  yields the expression for the stress distribution  $p = p_0 \cos \gamma(1 + 3(\Delta r/r) \sin^2 \gamma)$ , where the value of the ratio  $\Delta r/r$  is assumed to be small and the meaning of the symbols  $p_0$  and  $\gamma$  is the same as in Eq. (1) (Ipavec et al., 1997).

A recent analysis of the AP radiographs (Genda et al., 1995) by a computer simulation of the hip contact stress using a three-dimensional rigid body spring model showed that in dysplastic hips stress is concentrated at the anterolateral edge of the acetabulum and is increased with the reduction of the lateral coverage of the femoral head with the acetabulum which is in accordance with the above findings (Figs. 1–3) and the results of radiographic bone density studies (Pauwels, 1976). The superiorly located region corresponding to the maximal stress during stance period of gait determined in this work (Figs. 2 and 3) agrees well also with the theoretical predictions of Dalstra and Huiskes (1995).

Our analysis shows that in the cases where the pole lies outside the weight bearing area (Fig. 1B), the stress distribution on the weight bearing area steeply descends away from the border closest to the pole. It should be borne in mind that not only the value of  $p_{\max}$  is important for the loading of the hip but also the shape of the stress distribution (Brand, 1997). The value of  $p_{\max}$  may be relatively low if the body weight is low and if the articular sphere radius is large. The stress distribution may in spite of this be unfavorable if the pole lies outside the weight bearing area due to the steeply descending stress distribution (Fig. 1B).

## Appendix A. Towards the solution of Eq. (1)

To calculate the stress distribution in a given body position, the coordinate system is rotated with respect to the angle  $\vartheta$  for  $-\Theta$  so that the pole is at the top of the sphere. Further, the coordinate system is rotated with respect to the angle  $\varphi$  for  $-\Phi$ . The coordinates in the rotated system are denoted by the prime. The position of the pole in the rotated system is given by

$$\cos \Theta' = 1, \quad \sin \Phi' = 0. \quad (\text{A.1})$$

The force lies in the  $y' = 0$  plane while the weight bearing area lies in the rotated system above the  $z' = 0$  plane and is symmetric with respect to the  $y' = 0$  plane (Fig. 4).

Due to the symmetry of the weight bearing area with respect to  $y' = 0$  plane, the three-dimensional problem may be mapped onto two dimensions so that the coordinate of the pole  $\Theta$  can be ascribed also negative values.

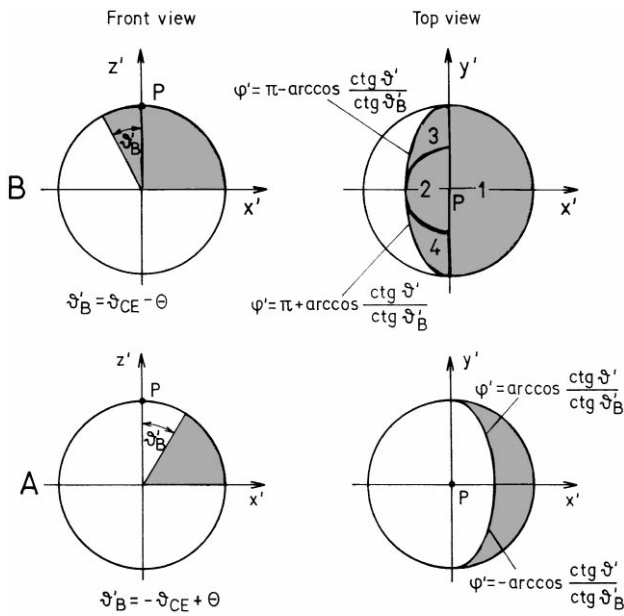


Fig. 4. The weight bearing area of the articular sphere (shaded) in the rotated system in the case when the pole lies on the lateral side outside the weight bearing area (A) or within the weight bearing area, but not further than for an angle  $\pi/2$  away from the lateral border of the weight bearing area (B). The front and the top views are shown. The expressions determining the lateral border of the weight bearing area are given in the top view. The location of the pole is indicated.

The angle  $\Theta$  is taken to be positive in the lateral direction, the angle  $\vartheta_R$  is taken to be positive in the medial direction, while the CE angle  $\vartheta_{CE}$  is taken to be positive in the lateral direction.

The lateral and the medial border are in the rotated system determined by the intersection of the sphere with the corresponding plane, this plane being inclined with respect to  $x' = 0$  plane by the respective angle  $\vartheta'_B$ . For the points on the borders, the ratio of the  $z'$  and  $x'$  coordinates is constant,

$$\frac{z'}{x'} = \text{ctg } \vartheta'_B. \tag{A.2}$$

Using the relations between the spherical and the Cartesian coordinates  $z' = r \cos \vartheta'$  and  $x' = r \cos \varphi' \sin \vartheta'$  and Eq. (A.2), the interdependence between the angle  $\varphi'$  and the angle  $\vartheta'$  on the respective border is obtained (Fig. 4)

$$\cos \varphi' = \text{ctg } \vartheta' / \text{ctg } \vartheta'_B. \tag{A.3}$$

The unknown spherical coordinates of the stress pole  $\Theta$  and  $\Phi$  and the value of stress at the pole  $p_0$  can be determined by solving a system of the three components of the vector equation (1). As in the rotated system the coordinate of the pole  $\Theta$  is zero (Eq. (A.1)), it follows from Eq. (A.3) that

$$\cos \gamma' = \cos \vartheta'. \tag{A.4}$$

Knowing the values of all three components of the resultant hip joint force in the rotated system and considering the expression for  $dS$ , the vector equation (1) in the component form in the rotated system is

$$p_0 r^2 \iint \cos \vartheta' \sin^2 \vartheta' \cos \varphi' d\vartheta' d\varphi' = R \sin(\vartheta_R + \Theta) \cos(\varphi_R - \Phi), \tag{A.5}$$

$$p_0 r^2 \iint \cos \vartheta' \sin^2 \vartheta' \sin \varphi' d\vartheta' d\varphi' = R \sin(\vartheta_R + \Theta) \sin(\varphi_R - \Phi), \tag{A.6}$$

$$p_0 r^2 \iint \cos^2 \vartheta' \sin \vartheta' r^2 d\vartheta' d\varphi' = R \cos(\vartheta_R + \Theta). \tag{A.7}$$

The integrals in Eqs. (A.5)–(A.7) can be calculated analytically due to the choice of the coordinate system in which the weight bearing area attains a simple shape. In performing the integrations the weight bearing area is divided into the segments (marked in Fig. 4) within which the integrals can be obtained analytically. The integral in Eq. (A.6) is zero in accordance with the notion that the component of the force in the  $y'$  direction is zero,

$$R \sin(\vartheta_R + \Theta) \sin(\varphi_R - \Phi) = 0, \tag{A.8}$$

implying the validity of Eq. (A.3). Expressions (A.5) and (A.7) yield after a lengthy procedure which is due to space limitations not presented Eqs. (5) and (6). Due to symmetry of the weight bearing area in the rotated system and the direction of the resultant hip force in the rotated system the integrals in Eqs. (A.5) and (A.7) solve out cleanly so that the obtained Eqs. (5) and (6) are relatively short.

**References**

Baker, K.J., Brown, T.D., Brand, R.A., 1989. A finite-element analysis of intertrochanteric osteotomy on stresses in femoral head osteonecrosis. *Clinical Orthopaedics and Related Research* 249, 183–198.

Brand, R.A., 1997. Hip osteotomies a biomechanical consideration. *Journal of the American Academy of Orthopaedic Surgeons* 5, 282–291.

Brand, R.A., Pedersen, D.R., Davy, D.T., Kotzar, G.M., Heiple, K.G., Goldberg, V.M., 1994. Comparison of hip force calculation and measurements in the same patient. *Journal of Arthroplasty* 9, 45–51.

Brinckmann, P., Frobin, W., Hierholzer, E., 1981. Stress on the articular surface of the hip joint in healthy adults and persons with idiopathic osteoarthritis of the hip joint. *Journal of Biomechanics* 14, 149–156.

Brown, T.D., Shaw, D.T., 1983. In vitro contact stress distributions in the natural human hip. *Journal of Biomechanics* 16, 373–384.

Brown, T.D., Pedersen, D.R., Baker, K.J., Brand, R.A., 1993. Mechanical consequences of core drilling and bone — grafting on osteonecrosis of the femoral head. *Journal of Bone and Joint Surgery* 75A, 1358–1367.

Buschmann, M.D., Grodzinsky, A.J., 1995. A molecular model of proteoglycan-associated electrostatic forces in cartilage mechanics. *Journal of Biomechanical Engineering* 117, 179–192.

- Byers, P.D., Hoaglund, F.T., Purewal, G.S., Yau, A.C.M.C., 1974. Articular cartilage changes in Caucasian and Asian hip joints. *Annals of the Rheumatic Diseases* 33, 157–161.
- Crowninshield, R.D., Johnston, R.C., Andrews, J.S., Brand, R.A., 1978. A biomechanical investigation of the human hip. *Journal of Biomechanics* 11, 75–85.
- Dalstra, M., Huiskes, R., 1995. Load transfer across the pelvic bone. *Journal of Biomechanics* 28, 715–724.
- Das De, S., Bose, K., Balasubramaniam, P., Goh, J.C.H., Teng, B., 1985. Surface morphology of Asian cadaveric hips. *Journal of Bone and Joint Surgery* 67B (2), 225–228.
- Genda, E., Konishi, N., Hasegawa, Y., Miura, T., 1995. A computer simulation study of normal and abnormal hip joint contact pressure. *Archives of Orthopaedics and Trauma Surgery* 114, 202–206.
- Greenwald, A., O'Connor, J.J., 1971. The transmission of load through human hip joint. *Journal of Biomechanics* 4, 507–528.
- Hadley, N.A., Brown, T.D., Weinstein, S.L., 1990. The effects of contact pressure elevations and aseptic necrosis on the long-term clinical outcome of congenital hip dislocation. *Journal of Orthopaedic Research* 8, 504–513.
- Hodge, W.A., Fijan, R.S., Carlson, K.L., Burgess, R.G., Harris, W.H., Mann, R.W., 1986. Contact pressures in the human hip joint measured in vivo. *Proceedings of the National Academy of Sciences of the USA* 83, 2879–2883.
- Hodge, W.A., Carlson, K.L., Fijan, R.S., Burgess, R.G., Riley, P.O., Harris, W.H., Mann, R.W., 1989. Contact pressures from an instrumented hip endoprosthesis. *Journal of Bone and Joint Surgery* 71A, 1378–2883.
- Iglič, A., Kralj-Iglič, V., Antolič, V., Srakar, F., Stanič, U., 1993. Effect of the periacetabular osteotomy on the stress on the human hip joint articular surface. *IEEE Transactions on Rehabilitation Engineering* 1, 207–212.
- Ipavec, M., Iglič, A., Kralj-Iglič, V., Antolič, V., 1997. Influence of nonspherical shape of the femoral head on the compressive stress in the hip joint articular layer. In: Zajc, B. (Ed.), *Proceedings of the 6th Conference of Slovenian IEEE Section*. University of Ljubljana, Ljubljana, pp. 351–354.
- Krebs, D.E., Elbaum, L., Riley, P.O., Hodge, W.A., Mann, R.W., 1991. Exercise and gait effects on in vivo hip contact pressures. *Physical Therapy* 71, 301–309.
- Kummer, B., 1991. Die klinische Relevanz biomechanischer Analysen der Hüftregion. *Zeitschrift für Orthopädie und ihre Grenzgebiete* 129, 285–294.
- Legal, H., Ruder, H., 1977. Zur biostatistischen Analyse des Hüftgelenks. *Zeitschrift für Orthopädie und ihre Grenzgebiete* 115, 215–234.
- Legal, H., Reinecke, M., Ruder, H., 1980. Zur biostatistischen Analyse des Hüftgelenks III. *Zeitschrift für Orthopädie und ihre Grenzgebiete* 118, 804–815.
- Maxian, T.A., Brown, T.D., Weinstein, S.L., 1995. Chronic stress tolerance levels for human articular cartilage: two nonuniform contact models applied to long term follow-up of CDH. *Journal of Biomechanics* 28, 159–166.
- Pauwels, F., 1976. In: *Biomechanics of the Normal and Diseased Hip*. Springer, Berlin.
- Rapperport, D.J., Carter, D.R., Schurman, D.J., 1985. Contact finite element stress analysis of the hip joint. *Journal of Orthopaedic Research* 3, 345–446.
- Rushfeldt, P.D., Mann, R.W., Harris, W.H., 1981. Improved techniques for measuring in vitro the geometry and pressure distribution in the human acetabulum — II. Instrumented endoprosthesis measurements of articular surface pressure distribution. *Journal of Biomechanics* 14, 315–323.
- Shrive, N.G., Frank, C.B., 1995. Articular cartilage. In: Nigg, B.M., Herzog, W. (Eds.), *Biomechanics of the Musculo-Skeletal System*. Wiley, Chichester, pp. 79–105.
- Wiberg, G., 1939. Studies on dysplastic acetabula and congenital subluxation of the hip joint — with special reference to the complication of osteoarthritis. *Acta Orthopaedica Scandinavica (Suppl.)* 58, 1–135.